Journal of Power Sources 195 (2010) 8322–8326

Contents lists available at ScienceDirect

Journal of Power Sources

journal homepage: www.elsevier.com/locate/jpowsour

Short communication

Pyroxene $LiVSi_2O_6$ as an electrode material for Li-ion batteries

Jiangfeng Ni[a,*], Yoshiteru Kawabe[b], Masanori Morishita[b], Masaharu Watada[b], Nobuhiko Takeichi[a], Tetsuo Sakai[a,*]

[a] National Institute of Advanced Industrial Science and Technology, Kansai Center, 1-8-31 Midorigaoka, Ikeda, Osaka 563-8577, Japan
[b] GS Yuasa Corporation, Nishinosho, Kisshoin, Minami-ku, Kyoto 601-8520, Japan

ARTICLE INFO

Article history:
Received 16 March 2010
Received in revised form 7 June 2010
Accepted 24 June 2010
Available online 1 July 2010

Keywords:
Lithium ion battery
Pyroxene
Electrode material
Electrochemical behavior
Synchrotron radiation XRD

ABSTRACT

Lithium vanadium metasilicate ($LiVSi_2O_6$) with pyroxene structure has been exploited as an electrode material for Li-ion batteries. Galvanostatic charge and discharge tests show that $LiVSi_2O_6$ is able to deliver a capacity of 85 mAh g^{-1} at 30 °C, and a high capacity of 181 mAh g^{-1} at 60 °C. The high capacity is believed to be due to the reactions of V^{3+}/V^{4+} and V^{2+}/V^{3+}redox couples, accompanied by the excess 0.42 Li^+ insertion into the lattice forming a Li-rich phase $Li_{1.42}VSi_2O_6$. High-energy synchrotron XRD combined with the Rietveld refinement analysis confirms that the electrochemical delithiation–lithiation reaction proceeds by a single phase redox mechanism with an overall volume variation of 1.9% between $LiVSi_2O_6$ and its delithiated state, indicating a very stable framework of $LiVSi_2O_6$ for Li^+ ions extraction–insertion.

1. Introduction

Recent rapid development of solar power, wind power and hybrid electric vehicles (HEVs) makes energy conversion and storage increasingly important [1,2]. The success of these new energy industries relies heavily on the secondary battery systems, particularly Li-ion batteries [3]. Although Li-ion batteries have been widely used in portable electronic devices such as laptops, digital cameras and mobile phones, their applications in high power and large-format energy storage systems have been severely hindered by the currently prevailing cathode material, $LiCoO_2$, which cannot meet the safety and cost requirement. To address this issue, a large number of materials based on XO_m (PO_4, SiO_4, BO_3, etc.) polyanion structures have been explored due to the decent redox potential and improved safety [4–8]. The strong covalent X–O bond of the XO_m polyanions not only enhances the M^{2+}/M^{3+} redox potential through an inductive effect, but also prevents the O atoms from releasing even in abused condition.

These polyanion materials, however, are generally electronic poor conductors which limit their full access to the theoretical capacity. Over the last decade, many attempts have been made to improve their conductivity by versatile strategies such as coating the particle with carbon [9], doping with exotic ions [10] or reducing the particle size [11]. With better safety and improved electrochemical property, the polyanion materials, particularly olivine $LiFePO_4$, have gradually found application in advanced lithium batteries for use in high energy and power system as required by HEVs [12]. Nevertheless, the relatively low capacity due to large-format weight and only one electron transfer upon the delithiation–lithiation process cannot meet the energy density requirement of HEVs [3]. For instance, currently the most promising material $LiFePO_4$ only shows a limited capacity of 170 mAh g^{-1}. The silicate counterparts, Li_2MSiO_4 (M = Fe, Mn), have the potential of a high capacity above 300 mAh g^{-1} (two electrons transfer, M^{2+}/M^{3+} and M^{3+}/M^{4+}), however, the capacity related to the second electron transfer is extremely difficult to realize in practical utilization [5,6].

To improve material capacity, it is desirable to make use of redox reaction involving more than one electron. Vanadium-based materials seem to be particularly promising, because vanadium possesses a series of valences ranging from 2+ to 5+, which enables a redox reaction involving maximum three electrons. Accordingly, many vanadium oxides have been explored, and some of them indeed show a high capacity delivery at around 200 mAh g^{-1}. These oxides, however, require a Li-containing anode, and they exhibit unstable cyclability due to structure evolution [13], which limits their scale-up applications in current Li-ion batteries. Due to improved cyclability and thermal stability, vanadium-based polyanions such as $Li_3V_2(PO_4)_3$ [14], Li_2VOSiO_4 [15], and $Li_5V(PO_4)_2F_2$ [16] have drawn considerable attention, however, most of them do not show favorable electrochemical behavior except $Li_3V_2(PO_4)_3$ [14].

* Corresponding authors. Tel.: +81 72 751 9611; fax: +81 72 751 9623.
E-mail addresses: jiangfeng.ni@aist.go.jp, jfengni@gmail.com (J. Ni), sakai-tetsuo@aist.go.jp (T. Sakai).

0378-7753/$ – see front matter © 2010 Elsevier B.V. All rights reserved.
doi:10.1016/j.jpowsour.2010.06.085

In this work we report a new lithium vanadium metasilicate ($LiVSi_2O_6$) as a potential electrode material for Li-ion batteries. The $LiVSi_2O_6$ material belongs to the family of pyroxene in which the Li^+ ion can be replaced by other alkaline metal ion, the Si^{4+} by Ge^{4+}, and the V^{3+} by Al^{3+}, Fe^{3+}, Mn^{3+}, etc. [17]. Because of intrinsic magnetic moment of $S = 1$, the $LiVSi_2O_6$ is better known for its magnetic properties [18]. Here for the first time we study its electrochemical properties, and demonstrate that it holds the potential as a promising electrode material for advanced Li-ion batteries.

2. Experimental

The $LiVSi_2O_6$ material is usually prepared via a ceramic route involving high temperature and long time. For instance, Satto et al. prepared $LiVSi_2O_6$ single crystals at 1100 °C for 96 h, while Pedrini et al. obtained $LiVSi_2O_6$ powder of 95% purity at 990 °C for 100 h [17,18]. Here we develop a high-energy ball-milling assisted ceramic approach, the synthesis process operates at 950 °C for a few hours. The detailed synthetic procedure is summarized as following. First, intermediates with average formula $LiSi_2O_{4.5}$ were prepared by annealing the stoichiometric mixture of Li_2CO_3 and SiO_2 at 730 °C for 12 h. Then stoichiometric $LiSi_2O_{4.5}$ and V_2O_3 were weighed and thoroughly mixed by a high-energy ball-milling facility (High G, Kurimoto). After treating at 950 °C for 5 h in H_2/Ar (10:90) mixture atmosphere, the product was ball milled again and heated at 950 °C for another 3 h. To improve the conductivity, the product was coated by 2 wt.% carbon by pyrolyzing a certain amount of citric acid at 600 °C [19]. It is worth noting that all experiments were carried out on the carbon-coated products unless otherwise stated.

The XRD measurement was conducted at the BL19B2 beam line of the synchrotron radiation facility SPring-8, Japan, as reported in previous publication [20]. A large Debye–Scherrer camera was used to detect the fine diffraction patterns, and the wavelength was calibrated to be $\lambda = 0.700$ Å by using CeO_2 as a standard. Prior to measurement, the sample powder was loaded into a glass capillary ($\varphi = 0.3$ mm) and sealed with glue in an Ar filled glove box to prevent contamination. The structural analysis was performed with the Rietveld method on the program Rietan-2000 [21]. SEM and energy dispersive X-ray spectroscopy (EDX) were performed on a JEOL JSM-6390 microscope equipped with a JED-2300 spectrometer. Raman spectroscopy was recorded using a RMP-320 (Jasco) spectrometer with Ar laser of 50 mW at 532 cm^{-1}.

The electrochemical measurements were carried out on a 2032 coin cell. The cathode composite consists of 70 wt.% carbon-coated $LiVSi_2O_6$, 15 wt.% ketjen black, and 15 wt.% polyvinylidene, with a typical material loading of 5 mg cm^{-2}. The 2032 coin cells were assembled in a dry room with a dewpoint below −60 °C. The anode is Li foil and the electrolyte is 1 mol L^{-1} $LiPF_6$ in ethylene carbonate/dimethyl carbonate (EC/DMC) (1:1 by volume). The cells were tested on a Battery Labo System program-controlled test system (Keisokuki Center) in the voltage range of 1.5–4.5 V.

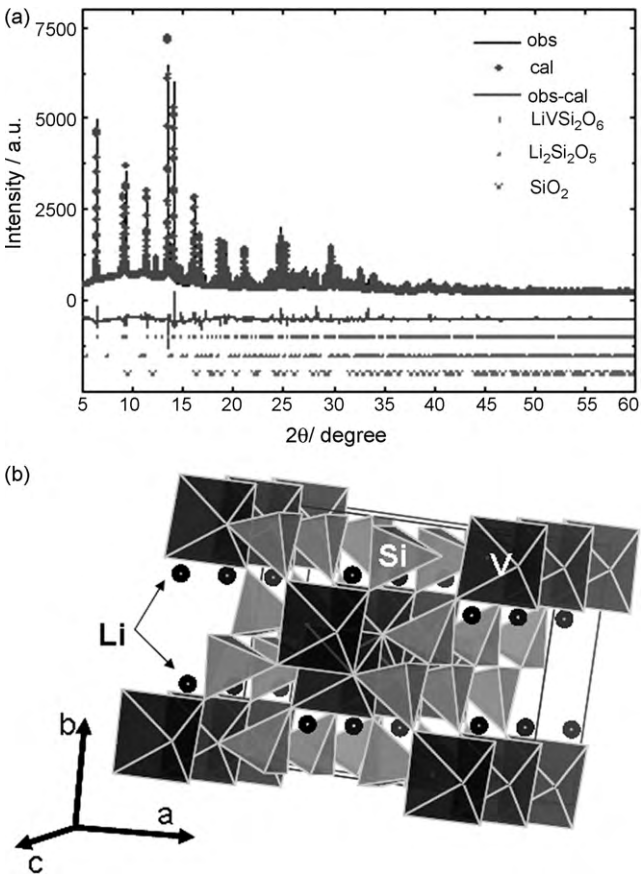

Fig. 1. (a) Rietveld refinement of the as-prepared $LiVSi_2O_6$. R_{wp}: 7.15%, R_p: 5.15%, S: 1.50. (b) Schematic representation of $LiVSi_2O_6$ pyroxene structure.

3. Results and discussion

Fig. 1a presents the synchrotron XRD pattern and its Rietveld refinement result of the as-prepared $LiVSi_2O_6$ material. The small difference between the observed pattern and the calculated one as well as the small value of factors R_{wp}, R_p, and S, verifies that the structural analysis is reliable. The XRD pattern is indexed as a major pyroxene phase (ICSD No. 159535), two minor impurities of $Li_2Si_2O_5$ (ICSD No. 280481) and SiO_2 (ICSD No. 083849) and the detailed structure information is listed in Table 1. The pyroxene phase crystallizes in a monoclinic structure, space group $C2/c$ (the same as $LiFeBO_3$ [6]) with resolved lattice parameters of $a = 9.6342(5)$ Å, $b = 8.6070(4)$ Å, $c = 5.3028(3)$ Å, $\beta = 109.62(2)^\circ$, and $V = 414.20$ Å^3, consistent with previous reports [17,18]. A high purity (96.6%) is confirmed by the phase abundance analysis, indicating the effectiveness of our synthesis strategy. This high purity is comparable with Pedrini's result (purity ~95%) [18], and our strategy is obviously more suitable because our preparation only takes a few hours instead of 100 h [18]. It is believed that the high-energy ball-milling process facilitates the intimate mixing of ingredients

Table 1
The structural parameters of the as-prepared $LiVSi_2O_6$ sample.

	Phase	S.G.	a (Å)	b (Å)	c (Å)	β (°)	V (Å^3)	Content (wt.%)
As-prepared	$LiVSi_2O_6$	$C2/c$	9.6342(5)	8.6070(4)	5.3028(3)	109.62(2)	414.20	96.6
	Li_2SiO_5	$Ccc2$	5.789(2)	14.60(3)	4.760(2)		402.42	2.6
	SiO_2	$P3_221$	4.936(3)	4.936(3)	5.40(1)		113.97	0.8
Charged (70% SOC)	$Li_{0.3}VSi_2O_6$	$C2/c$	9.5907(5)	8.5698(4)	5.2785(2)	109.62(2)	408.66	96.4
	Li_2SiO_5	$Ccc2$	5.793 (2)	14.60(2)	4.762(1)		402.69	2.7
	SiO_2	$P3_221$	4.932(3)	4.932(3)	5.40(2)		113.87	0.9

Table 2
The atomic parameters for $LiVSi_2O_6$ and its charged phase ($Li_{0.3}VSi_2O_6$). Here *g* is the site occupancy and *B* is the overall isotropic atomic displacement parameters.

Phase	Atom	Site	*x*	*y*	*z*	*g*	*B* (Å^2)
As-prepared	Li	4e	0	0.289(2)	0.25	1	0.5
	V	4e	0	0.908(1)	0.25	1	0.23(5)
	Si	8f	0.296(1)	0.089(2)	0.268(1)	1	0.32(3)
	O1	8f	0.116(3)	0.080(2)	0.152(1)	1	0.14(2)
	O2	8f	0.369(2)	0.255(1)	0.319(1)	1	0.36(2)
	O3	8f	0.348(2)	0.001(1)	0.053(2)	1	0.17(4)
Charged (70% SOC)	Li	4e	0	0.267(2)	0.25	0.3	0.5
	V	4e	0	0.906(1)	0.25	1	0.35(2)
	Si	8f	0.297(1)	0.090(1)	0.269(2)	1	0.29(4)
	O1	8f	0.114(2)	0.087(1)	0.157(1)	1	0.22(2)
	O2	8f	0.363(1)	0.256(1)	0.321(3)	1	0.34(5)
	O3	8f	0.352(2)	0.000(3)	0.052(1)	1	0.28(3)

and increases the reaction kinetics [22]. It is worth of noting that a second treatment at 950 °C is necessary to improve the purity, however, attempt to fully remove $Li_2Si_2O_5$ and SiO_2 impurities has not been achieved, which is reminiscent of other silicate materials like Li_2FeSiO_4 and Li_2MnSiO_4 [5,6].

The structure of pyroxene $LiVSi_2O_6$ is schematically presented in Fig. 1b, and the atomic parameters are also summarized in Table 2. In the crystalline the V^{3+} ions occupy the centers of the VO_6 octahedra, which form isolated edge-shared chains linked together by the SiO_4 tetrahedral to form a three-dimensional framework, while the Li^+ ions occupy the interstitial sites to form chains along *c*-axis direction. This three-dimensional framework allows Li^+ ions to move freely in the distorted octahedra, making $LiVSi_2O_6$ feasible as electrode material for Li-ion battery. However, a slow kinetics of Li diffusion may be expected, because the possible exchange distance for two adjacent Li ions are 0.449 nm (*bc* plane) and 0.470 nm (*ab* plane), respectively, which are much larger than that in the $LiFePO_4$ (~0.30 nm).

Fig. 2a shows the SEM image of $Li_2VSi_2O_6$ material. It is seen that the particles are mainly in the submicron range (200–500 nm) with an even size distribution, though some large agglomerates are also visible. The collection of EDX examination shown in Fig. 2b confirms the presence of V, Si, O and C, and an elemental mapping analysis (not shown here) reveals that their distribution is uniform.

To collect more structural information of the as-prepared $LiVSi_2O_6$, Raman spectroscopy measurement was performed on both bare $LiVSi_2O_6$ and carbon-coated one, and their spectra are presented in Fig. 3. Analogous to $LiFePO_4$, the vibration spectrum of $LiVSi_2O_6$ is dominated by SiO_4 tetrahedra, because the bond strength of SiO_4 group is much greater than other polyhedra like VO_6 and LiO_6 octahedra [23,24]. In the Raman spectrum of the bare $LiVSi_2O_6$, the bands around 1030 cm^{-1} and 860 cm^{-1} are related to asymmetric stretching vibration of Si–O, while the band in the 720–830 cm^{-1} can be assigned to the bending vibration of O–Si–O and Si–O–Si. The intensity of the latter band is somewhat high, which is related to SiO_2 impurity [24]. The weak band at 230 cm^{-1} is attributed to the external mode, which is difficult to be assigned to specific vibration because it is composed of the whole body translational and librational movement of the SiO_4 group and the metal ions V^{3+} and Li^+. In the spectrum of carbon-coated sample, the band intensity related to SiO_4 group decreases, while two additional strong bands centered at 1345 cm^{-1} and 1595 cm^{-1} emerge, which are the typical D band and G band of carbon, respectively [19].

The electrochemical property of the material was investigated using coin cells with Li foil as the counter electrode. Fig. 4a shows the typical galvanostatic charge and discharge profiles at 0.05 C (1 C = 127 mA g^{-1}) at 30 °C. A capacity of 85 mAh g^{-1} (equal to 0.67 Li per formula) is achieved over 1.5–4.5 V proceeding by a continuous sloping profile rather than plateau, indicative of a single phase process [25]. To better understand the galvanostatic process, the differential curve (d*Q*/d*V*) derived from the charge and discharge profile is also given in Fig. 4b. Three pairs of redox humps rather than sharp peaks at 2.19/2.00 V, 3.22/3.12 V, and 4.22/4.02 V are observed. These redox humps reflect different steps of Li diffusion from/into $LiVSi_2O_6$ crystals, which is related to a sluggish kinetics process. The exchange distance for Li^+ hopping is particularly long, and there is more than one potential direction for Li^+ movement (see Fig. 1b), so the Li diffusion may proceed by various steps distinguished by different driven forces (potentials). Similar phenomenon is also observed in other materials with poor kinetics like $LiFeBO_3$ [8]. It is expected that the particle size will affect the electrochemical performance to a large extent. Indeed, tests on another $LiVSi_2O_6$ power material with similar purity but with micron particles show that the discharge capacity is quite low, at only 40 mAh g^{-1}. Despite of the relatively low capacity, this sub-

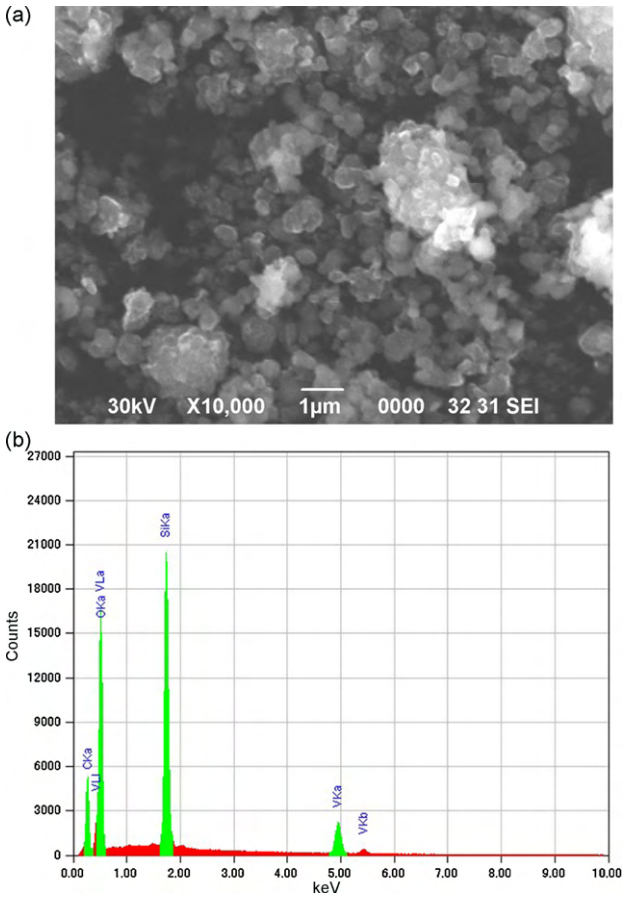

Fig. 2. SEM image (a) and EDX spectroscopy (b) of the as-prepared $LiVSi_2O_6$.

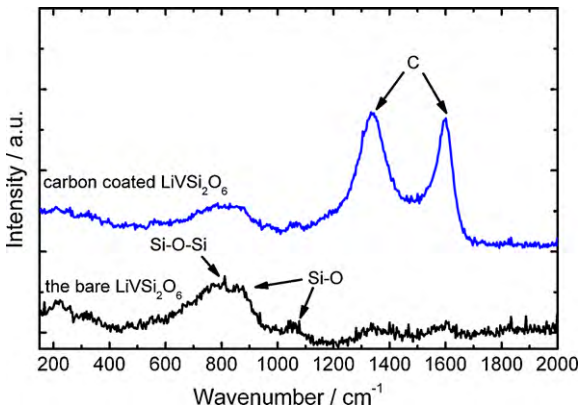

Fig. 3. Raman spectroscopy of the bare and carbon-coated $LiVSi_2O_6$.

micron material shows a favorable cyclability, as seen in Fig. 5. Upon repeating 40 cycles, the capacity does not fade but increases gradually to 96 mAh g^{-1}.

To understand the structure evolution over the electrochemical process, synchrotron radiation XRD and Rietveld refinement were also done on the charged electrode (70% state of charge (SOC)) after 20 cycles at 30 °C (Fig. 6). It is found the charged electrode exhibits almost a similar pattern to the fresh material except for slightly peak shift towards high angle, indicative of a single phase electrochemical behavior, in good agreement with the electrochemical analysis. Structural analysis on synchrotron radiation data was performed and some lattice and atomic parameters are listed in Tables 1 and 2, respectively. The Rietveld analysis releases

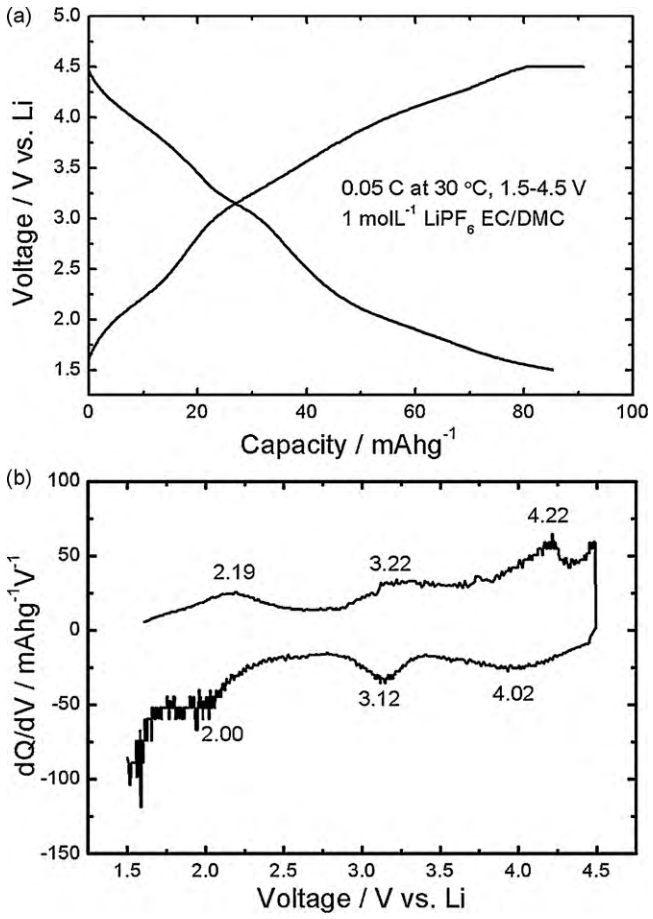

Fig. 4. (a) Charge and discharge profiles of $LiVSi_2O_6$ and (b) the corresponding differential curves.

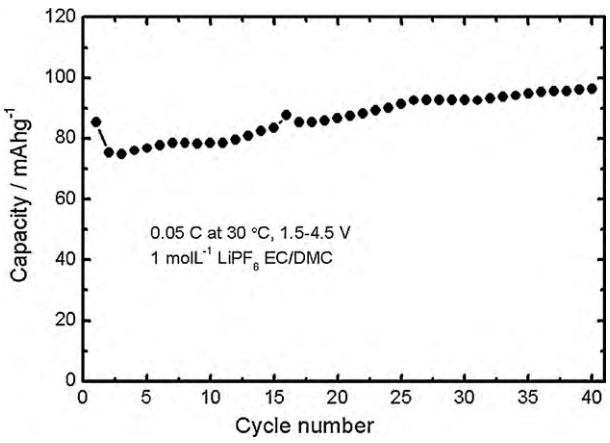

Fig. 5. Discharge capacity of $LiVSi_2O_6$ at 30 °C as a function of cycle number.

a slightly reducing parameters of $a = 9.5907(4)$ Å, $b = 8.5698(4)$ Å, $c = 5.2785(2)$ Å, $\beta = 109.62(2)°$, and $V = 408.66$ Å^3 (see Table 1). The overall 1.9% decrease in volume (extrapolated to 100% SOC) is even less insignificant than that of $LiFePO_4$ (6.5%) [4], which provides possibly explanation to the stable cycling behavior shown in Fig. 5.

Considering the fact that the silicate materials exhibit poor kinetics [5,6], galvanostatic tests were also operated at 60 °C. The coin cells were charged at a constant rate of 0.05 C and discharged at different rates. Fig. 7a presents the rate discharge curves of $LiVSi_2O_6$ at 60 °C. For clarification, the charge curves of the first two cycles are plotted as well. It is clearly seen that high temperature facilitates the Li^+ ions deintercalation–intercalation process. A high charge capacity of 126 mAh g^{-1} and, more surprising, a higher discharge capacity of 181 mAh g^{-1} (equal to 1.42 Li per formula) are observed in the first galvanostatic cycle, which indicates most Li^+ ions were extracted upon charge and 1.42 Li^+ ions per formula was re-inserted into $LiVSi_2O_6$ lattice upon discharge. The excess Li^+ ions might diffuse into the interstitial sites to form a Li-rich phase $Li_{1.42}VSi_2O_6$, while simultaneously partial V^{3+} ions were further reduced to V^{2+} ions. This result proves exactly that the capacity involving the second electron is accessible in pyroxene material, and that also adds weight to its competition with other electrode materials. Again, the plot of dQ/dV curve of the second cycle is drawn to better understand the electrochemical process (Fig. 6b). It is found that the dQ/dV curve at 60 °C is consistent with that at 30 °C, except for a somewhat shift of humps, indicative of a similar electrochemical mechanism at these two temperatures. A close examination reveals that the hump in the range of 1.8–2.3 V becomes much stronger,

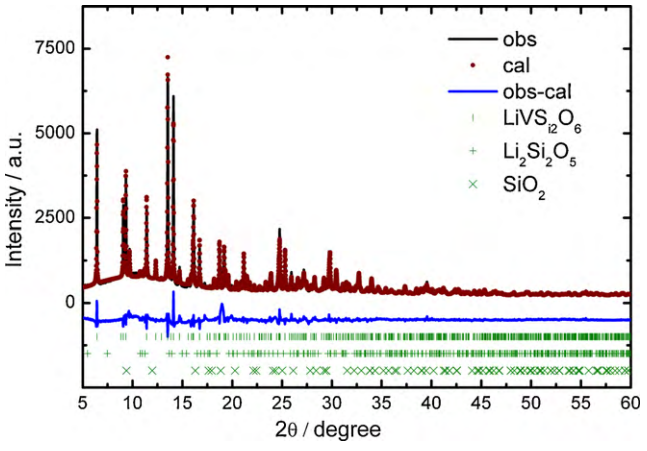

Fig. 6. Rietveld refinement of charged $LiVSi_2O_6$ electrode (70% SOC) after 20 cycles. R_{wp}: 6.87%, R_p: 4.24%, S: 1.45.

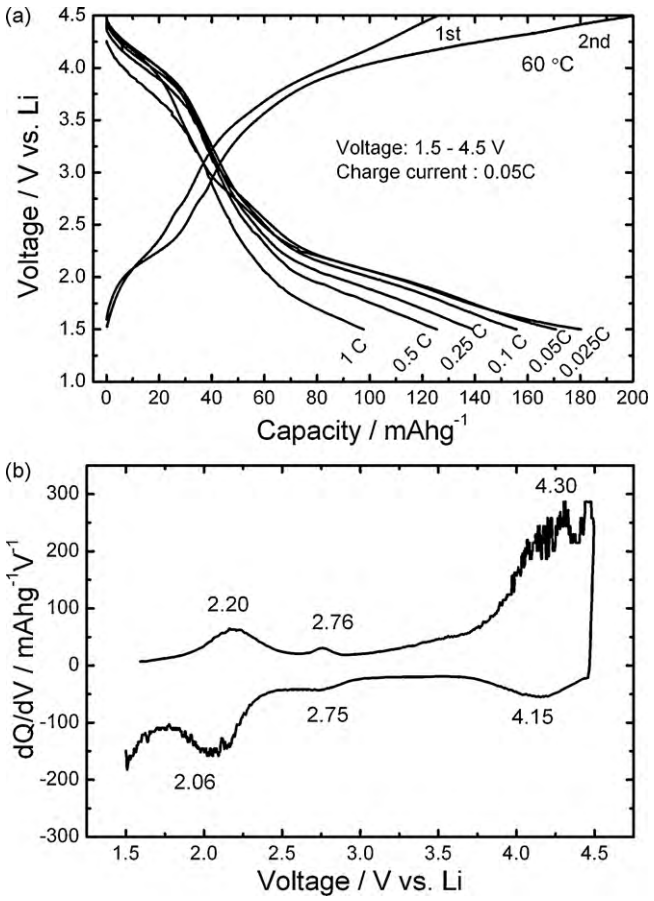

Fig. 7. (a) Rate discharge capability of $LiVSi_2O_6$ at 60 °C. The first and second charge curves are also plotted for clarification. Charge current rate: 0.05 C. (b) The differential curves corresponding to the second charge–discharge cycle.

which is probably associated with the accommodation of excess Li^+ ions. This assumption also can find evidence in the discharge curve, in which a large capacity was found over this range.

It is noted that the utilization of redox couple of V^{2+}/V^{3+} may need extra Li source, but this would not become a problem if integrating some "Li storage" materials like Li_5FeO_5 or Li_2MnO_3 [26]. Increasing the discharge rate, however, results in a remarkable decrease in the capacity, and only 98 mAh g^{-1} is obtained at 1 C rate. It is believed that the poor rate capability can be enhanced given that the material design like particle size and conductive coating is optimized [9,11]. The cycling behavior at 60 °C was further investigated. Fig. 8 shows the discharge capacity at 60 °C as a function of cycle number. It is seen that the cyclability is not as good as that at 30 °C, and only 127 mAh g^{-1} was delivered at the 20th cycle comparing with the initial 170 mAh g^{-1}. This capacity fading is primarily related to the deterioration of electrolyte/electrode interphase at high temperature, rather than to the structural deformation, and thus an effective coating layer will help to resolve this problem [27]. The coating experiment and the structural analysis of $Li_2VSi_2O_6$ after excess Li insertion by synchrotron XRD are currently undergoing, and the results will be reported in the future.

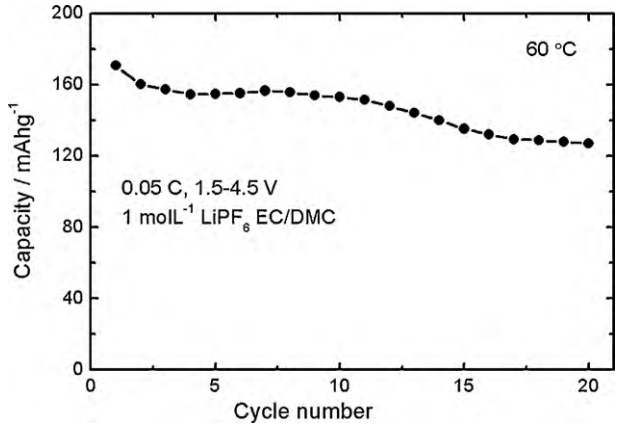

Fig. 8. Discharge capacity of $LiVSi_2O_6$ at 60 °C as a function of cycle number.

4. Conclusion

Highly pure $Li_2VSi_2O_6$ material was prepared by a modified ceramic approach with the assistance of high-energy ball-milling, and its electrochemical activity was investigated. At 30 °C, only 85 mAh g^{-1} was delivered involving the redox couple of V^{3+}/V^{4+}; at 60 °C, a high capacity of 181 mAh g^{-1} was observed involving the redox reactions of both V^{3+}/V^{4+} and V^{2+}/V^{3+}couples. The structural analysis of charged electrode material confirms that the material undergoes a single phase electrochemical delithiation–lithiation process, with an overall volume variation of 1.9% between $Li_2VSi_2O_6$ and its fully charged state. The results of this work demonstrate for the first time that pyroxene materials are promising cathode candidates for Li-ion batteries.

Acknowledgement

We thank two anonymous reviewers for their constructive suggestions.

References

[1] W.-Y. Wong, X.-Z. Wang, Z. He, A.B. Djurišić, C.-T. Yip, K.-Y. Cheung, H. Wang, C.S.K. Mak, W.-K. Chan, Nat. Mater. 6 (2007) 521.
[2] B. Hayman, J. Wedel-Heinen, P. Brøndsted, MRS Bull. 33 (2008) 343.
[3] M.S. Whittingham, Chem. Rev. 104 (2004) 4271.
[4] A.K. Padhi, K.S. Nanjundaswamy, J.B. Goodenough, J. Electrochem. Soc. 144 (1997) 1188.
[5] A. Nyten, A. Aboumrane, M. Armand, T. Gustafson, J.O. Thomas, Electrochem. Commun. 7 (2005) 156.
[6] Y.-X. Li, Z.-L. Gong, Y. Yang, J. Power Sources 174 (2007) 528.
[7] V. Legagneur, Y. An, A. Mosbah, R. Portal, A. Le Gal La Salle, A. Verbaere, D. Guyomard, Y. Piffard, Solid State Ionics 139 (2001) 37.
[8] Y.Z. Dong, Y.M. Zhao, Z.D. Shi, X.N. An, P. Fu, L. Chen, Electrochim. Acta 53 (2008) 2339.
[9] Y.G. Wang, Y.R. Wang, E. Hosono, K.X. Wang, H.S. Zhou, Angew. Chem. Int. Ed. 47 (2008) 1.
[10] H. Liu, Q. Cao, L.J. Fu, C. Li, Y.P. Wu, H.Q. Wu, Electrochem. Commun. 8 (2006) 1553.
[11] C. Delacourt, P. Poizot, S. Levasseur, C. Masquelier, Electrochem. Solid-State Lett. 9 (2006) A325.
[12] http://www.a123systems.com.
[13] M.S. Whittingham, Y. Song, S. Lutta, P.Y. Zavalij, N.A. Chernova, J. Mater. Chem. 15 (2005) 3362.
[14] H. Huang, S.-C. Yin, T. Kerr, N. Taylor, L.F. Nazar, Adv. Mater. 14 (2002) 1525.
[15] A.K. Parkash, P. Rozier, L. Dupont, H. Vezin, F. Sauvage, J.-M. Tarascon, Chem. Mater. 18 (2006) 407.
[16] Y. Makimura, L.S. Cahill, Y. Iriyama, G.R. Goward, L.F. Nazar, Chem. Mater. 20 (2008) 4240.
[17] C. Satto, P. Millet, J. Galy, Acta Cryst. C53 (1997) 1727.
[18] B. Pedrini, S. Wessel, J.L. Gavilano, H.R. Ott, S.M. Kavakov, J. Karpinski, Eur. Phys. J. B 55 (2007) 219.
[19] J. Ni, M. Morishita, K. Yoshiteru, M. Watada, N. Takeichi, T. Sakai, J. Power Sources 195 (2010) 2877.
[20] M. Morishita, T. Kakeya, S. Ochiai, T. Ozaki, Y. Kawabe, M. Watada, T. Sakai, J. Power Sources 193 (2009) 871.
[21] F. Izumi, T. Ikeda, Mater. Sci. Forum (2000) 321.
[22] C.W. Kim, J.S. Park, K.S. Lee, J. Power Sources 163 (2006) 144.
[23] C.M. Burba, R. Frech, J. Electrochem. Soc. 151 (2004) A1032.
[24] P. Makreski, G. Jovanovski, A. Gajović, T. Biljan, D. Angelovski, R. Jaćimović, J. Mol. Struct. 700 (2006) 102.
[25] M.Y. Saïdi, J. Barker, H. Huang, J.L. Swoyer, G. Adamson, Electrochem. Solid-State Lett. 5 (2002) A149.
[26] C.S. Johnson, M. Balasubramanian, S. Pol, S. Kang, M. Thackeray, Abstract 444, The 216th ECS Meeting, Vienna, Austria, October 4–9, 2009.
[27] J. Ni, H. Zhou, J. Chen, X. Zhang, Electrochim. Acta 53 (2008) 3075.